Article:
Hitaishi, VP, Mazurenko, I, Harb, M et al. (2018) Electrostatic-Driven Activity, Loading, Dynamics, and Stability of a Redox Enzyme on Functionalized-Gold Electrodes for Bioelectrocatalysis. ACS Catalysis, 8 (12). pp. 12004-12014. ISSN: 2155-5435

https://doi.org/10.1021/acscatal.8b03443

Electrostatic-driven activity, loading, dynamics and stability of a redox enzyme on functionalized-gold electrodes for bioelectrocatalysis

Vivek Pratap Hitaishi,[a] Ievgen Mazurenko,[b] Malek Harb,[a] Romain Clément,[a] Marion Taris,[c] Sabine Castano,[c] David Duché,[d] Sophie Lecomte,[c] Marianne Ilbert,[a] Anne de Poulpiquet,[a] Elisabeth Lojou*[a]

[a]*Aix-Marseille Univ, CNRS, BIP, UMR 7281, 31 Chemin Aiguier, 13009 Marseille, France*

[b] *School of Biomedical Sciences, University of Leeds, LS2 9JT Leeds, UK*

[c] *Institute for Chemistry and Biology of Membrane and Nano-objects, Allée Geoffroy St Hilaire, 33600 Pessac, France*

[d] *Aix Marseille Université, CNRS, Université de Toulon, IM2NP UMR 7334, 13397 Marseille, France*

ABSTRACT: **Oxygen reduction reaction is the limiting step in fuel cells, and many works are in progress to find efficient cathode catalysts. Among them, bilirubin oxidases are copper-based enzymes that reduce oxygen into water with low overpotentials. The factors that ensure electrocatalytic efficiency of the enzyme in the immobilized state are not well understood, however. In this work, we use a multiple methodological approach on a wide range of pH for protein adsorption and for electrocatalysis, to demonstrate the effect of electrostatic interactions on the electrical wiring, dynamics and stability of a bilirubin oxidase adsorbed on self-assembled-monolayers on gold. We show on one hand that the global charge of the enzyme controls the loading on the interface, and that the specific activity of the immobilized enzyme decreases with the enzyme coverage. On the other hand, we show that the dipole moment of the protein and the charge in the vicinity of the Cu site acting as the entry point of electrons, drive the enzyme orientation. In case of weak electrostatic interactions, we demonstrate that local pH variation affects the**

electron transfer rate as a result of protein mobility on the surface. On the contrary, stronger electrostatic interactions destabilize the protein structure and affect the stability of the catalytic signal. These data illustrate the interplay between immobilized protein dynamics and local environment that control the efficiency of bioelectrocatalysis.

KEYWORDS: *Enzymes; Catalysis; Self-Assembled-Monolayers; Electrochemistry; Ellipsometry; Surface Plasmon Resonance; PMIRRAS.*

INTRODUCTION

In an upcoming rising sustainable economy, fuel cells may play a role in the energy production. One of their limitations is the low efficiency of the oxygen reduction reaction (ORR), imposing the research of a catalyst combining high performance, stability and renewability [1-4]. Redox enzymes are such catalysts that efficiently operate in microorganisms to convert substrates. Among them, bilirubin oxidase (BOD), which belongs to the multi copper oxidase family, is one of the most considered alternative to platinum for oxygen reduction in enzymatic fuel cells [5-6]. The global catalytic cycle performed by this enzyme immobilized on electrochemical interfaces is now well established [5, 7]. It involves four copper centers, the CuT1 being the one which accepts the electrons from the reductant, and will therefore be the entry point of electrons from the electrode. Although enhanced catalytic performance has been achieved by entrapment of BOD in various carbon and metal nanomaterials [8-11], BOD-based bioelectrodes still suffer from low stability, precluding industrial use of the related biodevices. As an illustration, recent works in our laboratory showed that the half life of a BOD-based bioelectrode incorporated in carbon felts was restricted to one week at room temperature [12]. Furthermore, for direct wiring of a redox enzyme on a conductive support, it is mandatory to allow an electron tunneling between the enzyme active site and the electrode, and to permit substrate access [13-17]. By varying the pH of

BOD adsorption on a carbon nanotube (CNT) network, Mazurenko et al. demonstrated that electrostatic interactions were driving the adsorption process in an orientation favoring either this direct wiring (direct electron transfer, DET), or a connection via a diffusing redox mediator (MET) [15]. However, even after having defined the surface chemistry required for an efficient direct wiring, it was calculated that less than 10 % of the loaded enzymes were effectively participating to the catalysis [12]. Similar low percentage of electroactive enzymes was reported recently for laccase, another multicopper protein, on amorphous carbon nitride [18].

Understanding the factors that affect this low catalytic efficiency is thus required. While porous electrodes may enhance the loading of enzymes, planar electrodes are much more appropriate for the fundamental studies of enzyme immobilization [14, 19-22]. In particular, planar gold surfaces are mostly used in methods allowing to study loading of enzymes on solid supports (surface plasmon resonance (SPR), quartz crystal microbalance (QCM)), or enzyme conformation in the immobilized state (Surface-Enhanced Infrared Absorption (SEIRA), Surface-Enhanced Raman Spectroscopy (SERS), Polarization Modulation Infrared Reflection Adsorption Spectroscopy (PMIRRAS)) [14, 23-24]. Coupling these methods to electrochemistry is utmost crucial to be able to correlate electroenzymatic activity to enzyme amount and conformation, and to study the dynamics of the immobilized enzyme, with the ultimate goal of proposing bioelectrode rationalization [25]. Self-assembled-monolayers (SAMs) appear as fine tools allowing to easily tune and control the chemistry and charge of a planar gold electrochemical interface, while being rid of the complex surface chemistry and porosity of nanomaterials, which could influence the electrochemical response. Varying the pH may offer the additional advantage of changing the interactions between the surface and the enzyme by affecting both components in a controllable manner. However, the dynamics of the immobilized enzyme upon local pH change in the course of electrocatalysis has been rarely

investigated. One can cite the study by Jin et al. who investigated the pH-dependent interfacial electron transfer of cytochrome *c* electrostatically bound to a SAM [26].

In this work we bring new insight towards the comprehensive enzyme immobilization by the unprecedented coupling of electrochemistry to SPR, PMIRRAS and ellipsometry. *Myrothecium verrucaria* BOD (*Mv* BOD) adsorption on negative and positive SAM layers on gold electrodes was explored. Both the pH of adsorption and the pH for electrocatalysis were systematically varied to modulate the charge of the SAM-gold electrode, the global charge of the protein and the CuT1 vicinity charge. Modeling of cyclic voltammetry curves as well as analysis of DET and MET processes gave access to the distribution of enzyme orientations and enzyme dynamics as a function of pH conditions. Cyclic voltammetry was combined to SPR, PMIRRAS and ellipsometry to correlate the loading and conformation of the biomolecules on the surface to their activity, giving access to a specific activity of the immobilized enzyme. Finally, electrocatalysis at different applied potentials as a function of pH was investigated to prove the effect of electric field on the stability of the bioelectrode. The key parameters obtained for enzyme functional immobilization on planar electrodes will allow determining the next mandatory steps for the development of efficient biotechnological devices.

EXPERIMENTAL SECTION

Chemicals and materials. Ethanol analytical grade 96% (v/v), 2,2′-azino-bis(3-ethylbenzothiazoline-6-sulfonic acid) (ABTS), 6-mercaptohexanoic acid (6-MHA), 4-aminothiophenol (4-ATP), 11-mercaptoundecanoic acid (11-MUA), sodium hydroxide 97 % (NaOH) and sulfuric acid 95-98 % (H_2SO_4) were purchased from Sigma-Aldrich. Phosphate-Citrate (for pH 3.6 and 4.6) and phosphate (for pH above 5) buffer solutions were prepared by mixing Na_2HPO_4, NaH_2PO_4 and citric acid in an appropriate ratio to obtain pH in the range 3.6−7.5 and a final buffer concentration of 0.1 M. All solutions were prepared with Milli-Q water (18.2 MΩ cm). Bilirubin oxidase from *Myrothecium*

verrucaria (*Mv* BOD) was a gift from Amano Enzyme Inc. (Nagoya, Japan). Fresh solutions of *Mv* BOD were prepared in 100 mM phosphate, or phosphate-citrate buffers at the desired pH.

Electrode Preparation. A polycrystalline gold electrode (with a geometric surface of 0.008 cm^2) from Bio-Logic Science Instruments was used. Prior to use, the Au electrode was mechanically polished with 1.0, 0.3, and 0.05 μm Al_2O_3 slurry, subsequently followed by intermediate washing with Milli-Q water. After polishing, the electrode was electrochemically cleaned by cycling the applied potential between 0 and 1.35 V in 0.5 M H_2SO_4 at a scan rate of 100 $mV.s^{-1}$ until a stable voltammogram was obtained (~40 cycles). The electroactive surface area was calculated by integrating the gold oxide reduction peak, taking into account a charge of 390 $\mu C.cm^{-2}$ for the reduction of gold oxide monolayer. The roughness factor, R_f, defined as the ratio of electroactive surface area to projected geometrical surface area ($R_f = A_{electroactive} / A_{geometric}$), was determined for each electrode. Values between 2.7-3.2 are determined, allowing to calculate the real electroactive surface. All the currents in this work are reported versus this electroactive surface. Then, the Au electrode was sonicated with 1:1 (water-ethanol) solution for 10 min and rinsed twice extensively with water and later with ethanol. Finally, SAMs were formed by incubating the pretreated electrode in 5 mM ethanolic thiol solutions for 15±5 hours. The SAM modified electrodes are named according to the thiol molecule, i.e. 6-MHA-SAM, 4-ATP-SAM, etc. The surface was then cleaned with ethanol to remove all organic contaminants, and finally washed with water and dried under nitrogen flux. Prior to the enzyme immobilization, one CV cycle was done as a blank for thiol-SAM electrode. A reproducible voltammogram at 5 $mV.s^{-1}$ with capacitive current in the range 0.04-0.06 $\mu A.cm^{-2}$ was observed which reflects that the Au electrode surface is well decorated by thiol molecules.

pH dependent electrochemical response from adsorbed enzyme on thiol-SAM modified gold electrode was realized by following two independent approaches. The first approach was based on the enzyme adsorption at different pHs on thiol-SAM electrodes. Unless otherwise indicated the thiol-SAM electrode was incubated in 20 μM *Mv* BOD solution at the desired pH for 15 min at 4°C. This bioelectrode is named as thiol-SAM/*Mv* BOD. Then the thiol-SAM/*Mv* BOD electrode was removed from enzyme solution, gently washed with the same buffer to remove the loosely adsorbed enzymes,

and transferred to the electrochemical cell containing enzyme free phosphate buffer (100 mM) saturated with O_2 at a fixed pH 6 as a supporting electrolyte solution for electrocatalysis experiments. In another approach, a thiol-SAM/*Mv* BOD electrode was prepared by incubating a thiol-SAM electrode in 20 µM *Mv* BOD solution of fixed pH (100 mM buffer concentration) for 15 min at 4°C. After washing, the thiol-SAM/*Mv* BOD electrode was transferred to the electrochemical cell containing 100 mM buffer of variable pH as supporting electrolyte solution for electrocatalysis experiments.

Electrochemistry measurements. All electrochemical measurements (Cyclic voltammetry (CV), chronoamperometry and electrochemical impedance spectroscopy) were performed in a standard 3-electrode cell (comprising a polycrystalline gold as a working electrode, a Hg/Hg_2SO_4 reference electrode and a Pt-wire auxiliary electrode) using a potentiostat from Autolab PGSTAT30 controlled by Nova software (Eco Chemie). All potentials are quoted vs Ag/AgCl reference electrode by adding 430 mV to the measured potential. The cell was thermostated at 25°C and oxygen was continuously bubbled into the cell throughout the experiments, unless otherwise specified. No significant differences in magnitude and shape of catalytic curves were observed when varying the scan rate (Figure S1), suggesting that the voltammograms are close to the steady-state. At least three to five experiments were conducted in each condition, and only the bioelectrodes whose output current deviation was less than 10% of the average were considered. After DET signal was recorded, 50 µM ABTS was introduced in the solution to detect any MET process. The MET contribution was evaluated by the ratio between DET and (DET+MET) current.

Modeling of the cyclic voltammetry curves. The fitting of electroenzymatic curves was obtained by following the formalism developed by Armstrong and co-workers [27]:

$$j = \frac{j_{\lim}}{\beta d_0}\frac{e_1 - e_2}{1 + e_1}\ln\frac{pe_1^{\alpha_c} + (1 + e_1)}{pe_1^{\alpha_c} + (1 + e_1)\exp(-\beta d_0)} \quad (1)$$

Where $e_1 = \exp((n_1F/RT)(E - E^0_{CuT1}))$, $e_2 = \exp((-n_2F/RT)(E^0_{CuT1} - E^{eqm}_{O2/H2O}))$, $p = (k_{2a} + k_{2c})/k_{max}$. E^0_{CuT1} is the redox potential of the CuT1, $E^{eqm}_{O2/H2O}$ is the equilibrium potential of the O_2/H_2O redox

158 couple, n_1 and n_2 are the numbers of electrons transferred in the electrochemical and enzymatic
159 reactions respectively, and βd_0 is the dispersion parameter. The parameter p describes how proficient
160 the enzymatic electrocatalysis relative to interfacial transfer rate is. The background was subtracted
161 from the CVs prior to the fitting, and Origin 8.5 software was used for the fitting of the half CV cycle
162 within the potential window 0.6-0.1 V vs Ag/AgCl. For the different set of experiments E^{eqm}, was
163 adjusted according to the working electrolyte pH whatever the conditions of adsorption.
164
165 **Spectroscopic assays and protein aggregation measurements.** UV−vis absorption spectra were
166 recorded with a Cary-Win UV spectrophotometer equipped with a Peltier thermostable multicell
167 holder. All spectroscopic data were obtained with *Mv* BOD in phosphate/phosphate-citrate buffer (100
168 mM) at the desired pH. Same batch of enzyme was prepared and kept at either 4°C or 25°C. In a 500
169 µL clean cuvette, 10 µL of 200 nM enzyme, 50 µL of 20 mM ABTS and 430 µL of desired buffer
170 were mixed. Then UV-vis spectra were recorded for 60 s. The effect of pH on the BOD activity was
171 examined spectrophotometrically by following the oxidation of ABTS at 420 nm (ε_{420nm} = 36 mM^{-1}
172 cm^{-1}). All experiments were performed in triplicate, and standard errors were calculated. The mean of
173 the highest activity was set as 100% of the relative activity.
174 The aggregation measurements were done using UV-vis spectrophotometry. *Mv* BOD was diluted in
175 phosphate/phosphate-citrate buffer at the different pHs to 20 µM concentration. After 15 minutes
176 incubation at room temperature (RT) or in ice, UV-vis spectra were recorded. Apparition of aggregates
177 was followed overtime by measuring UV-vis absorption at 360 nm at RT.
178
179 **Surface Plasmonic Resonance (SPR).** SPR measurements were acquired on an Autolab SPRINGLE
180 instrument (Eco Chemie, The Netherlands) by using gold disks (25 mm diameter) purchased from Eco
181 Chemie. The thiol modification of the gold disks followed the same procedure as for the Au electrode.
182 For the SPR measurements, 100 µL of 0.1 M phosphate/phosphate-citrate buffer of desired pH, was
183 injected into the cell until stabilization of the signal was achieved. The buffer solution was then
184 replaced by a solution of 20 µM *Mv* BOD in buffer of desired pH, and the SPR signal was monitored
185 to follow enzyme adsorption at RT. At the end of the adsorption process, enzymes remaining in

solution and loosely adsorbed molecules were removed from the cell by buffer washing. The procedures for sample injection and removal were carried out using an autosampler (Eco Chemie) equipped with a peristaltic pump.

Data were analyzed by a SPR software from Eco Chemie. The mass of the adsorbed species was calculated from the SPR signal on the basis of the relation that a change of 122 mdeg (millidegrees) corresponds to 1.0 $ng.mm^{-2}$ at 25°C. For *Mv* BOD, this means that 100 mdeg of SPR angle corresponds to a coverage of 1.7 $pmol.cm^{-2}$. At least four experiments were conducted, and only the electrodes whose surface coverage deviation did not exceed 10% of the average were used. The standard deviation was calculated from the measurements using different electrodes. The mass of the adsorbed species was calculated from the SPR signal on the basis of the relation that a change of 122 mdeg (millidegrees) corresponds to 1.0 $ng.mm^{-2}$ at 25°C.

Ellipsometry. Variable Angle Spectroscopic Ellipsometry (VASE) has been performed in order to determine the thicknesses of the 6-MHA and 4-ATP based SAMs and the *Mv* BOD layers as a function of pH. We used a Semilab rotating compensator ellipsometer (RCE) with a microspot which focuses the beam on the sample. The beam diameter is around 100 µm. Data were measured for wavelengths ranging between 350 nm to 600 nm at three different incident angles (65°, 70° and 75°). The Ellipsometry Analysis (SEA) software from the Semilab company was used to fit the VASE measurements and to extract the dielectric functions $\varepsilon(\lambda)$ of the materials. This software allows minimizing the mean squared error (MSE) between the measured and the calculated ellipsometric spectra of $\tan(\Psi)$ and $\cos(\Delta)$ thanks to a Levenberg-Marquardt algorithm. Good agreement between the measurements and the calculations were obtained for all incident angles which indicates that the dispersion models are robust and appropriately fits the data. The obtained RMSE from the fits over the whole spectral range and for all incident angles ranges between 0.01 and 0.018 for all samples.

The dielectric function of gold has been fitted using Drude-Lorentz oscillators combined with a Sellmeier model. Drude-Lorentz oscillators are suitable for the dielectric constant determination of metals [28]. A Sellmeier model has been added in order to take into account the presence of H_2O molecules in the gold porosities when the substrates are introduced in the solutions. The dielectric

function of each gold substrate has been determined since it can weakly change from a sample to another one. The same dielectric function model has been used for the 6-MHA based SAMs and the *Mv* BOD layers. A Sellmeier model has been used to describe such non absorbing dielectric materials. The obtained refractive index is quasi-constant around 1.48 as a function of the wavelength which is very close to a previously reported value (n=1.45) [29].

For the VASE measurements, the samples were first plunged overnight in the thiol solutions in order to self assemble the 6-MHA monolayers on gold, then in the enzyme solution to adsorb the *Mv* BOD on the 6-MHA-SAM at 4°C for 15 min. Then, the samples were washed with buffer, then with water. Finally, the samples were carefully dried under mild nitrogen flux before performing the VASE measurements in air. The thickness was measured at three different positions on the sample. The thicknesses of the 6-MHA-SAM and 4-ATP-SAM were measured as 0.7±0.05 nm and 0.72±0.06 nm, respectively.

PMIRRAS measurements. Gold mirrors from Optics Balzers were used for PMIRRAS measurements. SAMs were formed by incubating the gold mirrors in 5 mM ethanolic thiol solutions for one night. The surface was then cleaned with ethanol to remove all organic contaminants, and finally washed with water and dried under nitrogen flux. The thiol-SAM functionalized gold surface was incubated in 20 µM *Mv* BOD solution at 4°C and at the desired pH for 15 min. To evaluate the effect of pH on the conformation of the immobilized enzyme, the thiol-SAM/*Mv* BOD gold surface was immersed in various pH buffers during 15 min.

For PMIRRAS analyses, the surface was cleaned with milli-Q water to remove salts present in the buffer, and finally the surface was dried. The modified dried gold electrode was placed at RT in the external beam of a Nicolet Nexus 870 FT-IR spectrometer (Madison, WI), and the reflected light was focused on a nitrogen-cooled (77 K) HgCdTe (MCT) detector (SAT, Poitiers). The optimal value of the angle of incidence for the detection was 75° relative to the optical axis normal to the interface. A ZnSe polarized grid and a ZnSe photoacoustic modulator to modulate the incident beam between p and s polarizations were placed before the sample. The detector output was sent to a two-channel

electronic device that generated the sum and the difference interferograms. The PMIRRAS spectra were recorded at 8 cm^{-1} resolution, with coaddition of 600 scans. Using a modulation of polarization enabled us to perform rapid analyses of the sample after treatment in various solutions without purging the atmosphere or requiring a reference spectrum. Protein adsorption can be attested by the presence of the amide I (mainly C=O stretching vibrational mode) and the amide II (mainly N-H stretching vibrational mode) at around 1660 and 1540 cm^{-1}, respectively [16]. Subtraction of the thiol-SAM spectra from the thiol-SAM/*Mv* BOD was realized for PMIRRAS data analysis.

RESULTS AND DISCUSSION

SAMs and *Mv* BOD charges as a function of pH. Four different pHs were used throughout this work: 3.6, 4.6, 6 and 7.5. In this pH range, both the protein and the electrode charges vary. Concerning *Mv* BOD, the theoretical global charge of the protein is slightly positive (+10) at pH 3.6, almost neutral at pH 4.6, and negative at the other pHs [15]. We calculated in this work a dipole moment around 800 Debye for the protein at pH 7.5, 6 and 4.6, while the value of the dipole moment decreases to less than 500 Debye for pH 3.6. The direction of the dipole moment points towards the CuT1 at pH 7.5 and pH 6, while its direction is shifted at pH 4.6 (Figure 1A). From our previous work, the charge in a sphere of 15 Å around the CuT1 is neutral at pH 7.5, slightly positive at pH 6 (+2) and displays a net positive value at pH 4.6 and 3.6 [15]. Both charge distributions are important for *Mv* BOD adsorption. The protein global charge is expected to control the repulsive or attractive interaction between the enzyme and the electrode, i.e. the strength of adsorption, while the local charge around the CuT1 may control the orientation of the protein for DET. Two types of thiol-based SAMs were investigated in this work to tune the electrostatic interactions (Figure 1B): 6-MHA and 11-MUA both carry carboxylic end-functions, and 4-ATP carries an amino group. As a function of pH, these SAM electrodes will present either positive, or negative or neutral charges depending on the pKa of the chemical end-function [30].

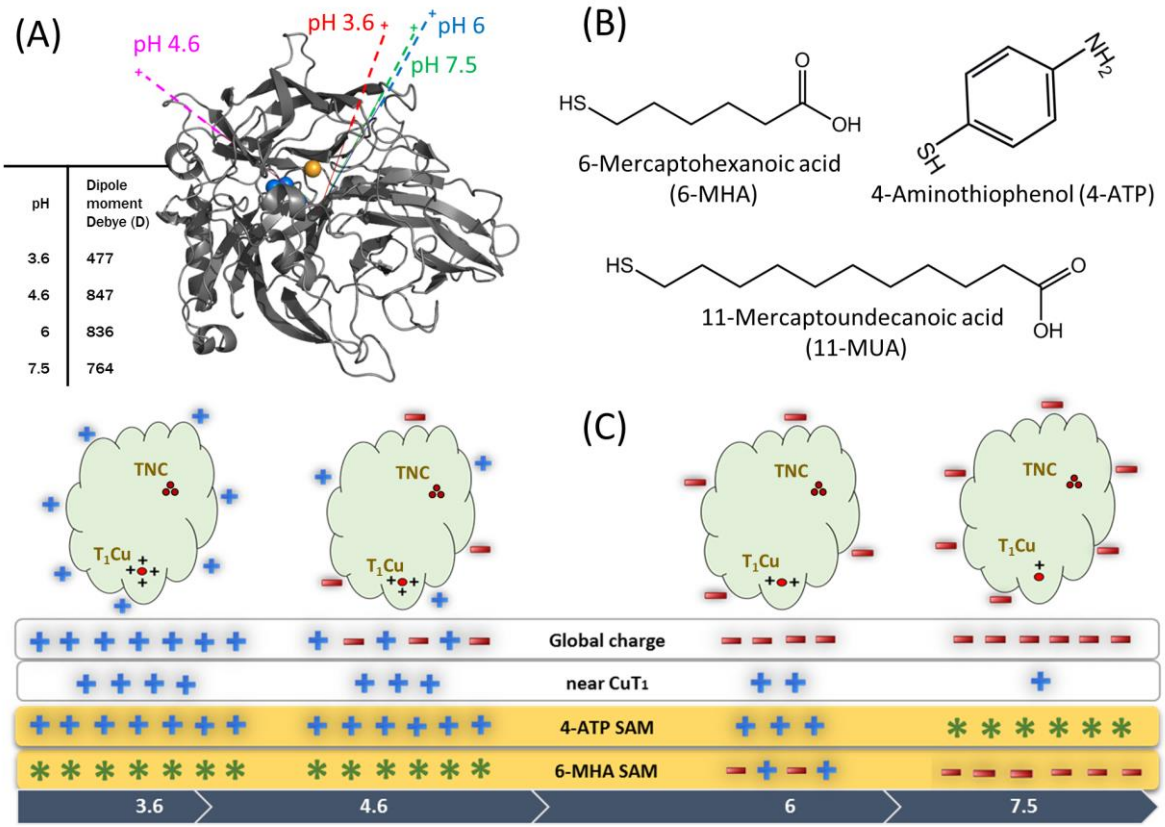

Figure 1. **Charges of *Mv* BOD and of the thiol-based SAMs as a function of pH.** (A) *Mv* BOD structure and dipole moments at pH 7.5, 6, 4.6 and 3.6. Blue spheres correspond to copper atoms involved in the trinuclear center, and the gold sphere corresponds to the CuT1. Dipole moments are calculated with Protein Dipole Moments Server [31], from structure prepared at different pHs with the PDB2PQR-Propka Server [32] using the Parse force fields. Illustration is performed with Pymol (The PyMOL Molecular Graphics System, Version 1.8 Schrodinger, LLC); (B) Formula of 6-MHA, 11-MUA, and 4-ATP; (C) Scheme illustrating the global charge of the *Mv* BOD enzyme, the charge around the CuT1 and the charges of 6-MHA-SAM and 4-ATP-SAM electrodes, as a function of pH. Green stars represent a neutral surface.

The pKa of thiols involved in SAMs is a function of the number of carbons forming the linear chain [33]. The pKa of 4-ATP was previously determined to be 6.9 [34]. In the case of the carboxylic terminated alkanethiols, it is known that the pKa of the surface thiols is higher than in solution as a result of the interactions between the thiol molecules in the SAM. The pKa of

11-MUA-SAM was reported to be around 6 [26]. In this work, we determined by impedance spectroscopy a pKa value close to 6 for 6-MHA-SAM (Figure S2). According to the statement made above, the comprehensive Figure 1C allows to envision pH zones for repulsive or attractive interactions between the enzyme and the SAM layer expected to control enzyme loading. It also permits to predict pH zones for which orientation of the protein for DET is expected to be favored as a function of the SAM chemistry.

Influence of the pH of adsorption of *Mv* BOD on 6-MHA-SAM. *Mv* BOD adsorption was carried out at 4°C on 6-MHA-SAM at the 4 different pHs, while recording the electroactivity at pH 6 and 25°C. Following this protocol, the intrinsic activity of enzymes adsorbed on SAM is fixed during the electrochemical experiments. The CV responses should have a direct dependence on enzyme loading and on the enzyme-SAM/enzyme-enzyme interactions that come into play at the electrochemical interface, both during the adsorption step and upon transfer to pH 6. Not only DET but also MET were quantified for each pH of adsorption. In addition, SPR and ellipsometry measurements as well as PMIRRAS spectra were recorded after enzyme adsorption at the four different pHs, to correlate the activity with the amount and conformation of the enzymes (Figure 2).

Independently of the pH of adsorption, DET occurs when the bioelectrode is transferred from a given pH to pH 6 (Figure 2A and Figure 2B). A sigmoidal wave develops in the presence of O_2, with an onset potential around 0.55 V suggesting a catalysis driven by the CuT1 [15-16]. The value of DET current density depends however on the pH of adsorption in the range: I_{DET} pH 3.6 < I_{DET} pH 7.5 < I_{DET} pH 4.6 ≈ I_{DET} pH 6. The DET current did not show any drastic variation between 1 and 15 min of adsorption, except for pH 3.6 where it is twice less after 15 min of adsorption compared to 1 min of adsorption. The CV shapes and modeling indicate

that enzyme orientation distribution on 6-MHA-SAM is more or less identical irrespective of the adsorption pH, with βd_0 values close to 5 (Figure 2C and Table 1).

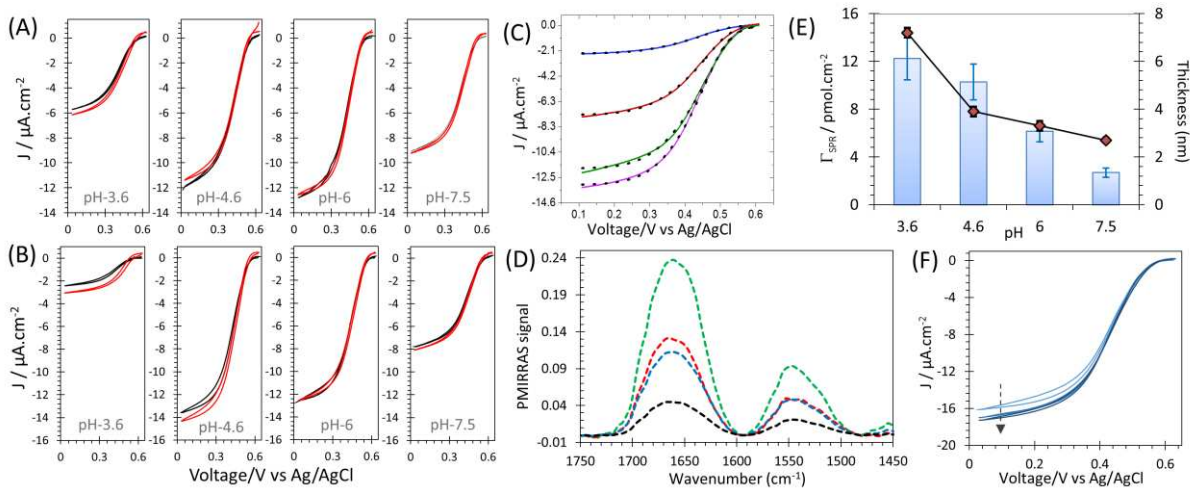

Figure 2. Correlation between electroactivity, orientation, conformation and loading of *Mv* BOD adsorbed at different pHs on carboxylic-based-SAMs. CVs of O_2 reduction at pH 6 and 25°C by *Mv* BOD adsorbed on 6-MHA-SAM at different pHs at 4°C after (A) 1 min and (B) 15 min of adsorption. Black lines and red lines are obtained before and after 50 µM ABTS addition in solution, respectively. 0.1 M phosphate buffer, v = 5 $mV.s^{-1}$. (C) Modeling of the electrochemical signal. Electrocatalytic CV curves at pH 6 obtained at different adsorption conditions (solid line) and curves fitted according to equation 1 (See experimental section) (dotted line): pH 3.6 (blue), pH 4.6 (purple), pH 6 (green), pH 7.5 (red). (D) PMIRRAS spectra of *Mv* BOD adsorbed on 6-MHA-SAM. The gold modified surface was placed in 20 µM *Mv* BOD solution at pH 7.5 (black line), pH 6 (blue line), pH 4.6 (red line) and pH 3.6 (green line) during 15 min and was then immersed in phosphate buffer at pH 6 during 30 min at 4°C. The gold modified electrodes were rinsed and dried in order to record PMIRRAS spectra. (E) Enzyme coverage and enzyme layer thickness as a function of pH after adsorption of 20 µM *Mv* BOD at RT during 15 min on 6-MHA-SAM. Enzyme coverage (blue bars) was obtained by SPR and enzyme layer thickness (◆) was measured by ellipsometry. (F) Increase in the consecutive CV catalytic currents at pH 6 after adsorption of 20 µM *Mv* BOD on 6-MHA-SAM in pH 4.6 buffer for 15 min at 4°C.

The amide I/amide II ratio on the PMIRRAS spectra is also the same whatever the pH (i.e. 3.2 ± 0.1, 3.1 ± 0.1, 3.0 ± 0.2, 2.9 ± 0.6 at pH 3.6, 4.6, 6 and 7.5 respectively) (Figure 2D). However, we already reported that the distribution and orientation of structural components in *Mv* BOD could yield to similar amide I/amide II ratio despite different orientations in the immobilized state [16]. ABTS as a redox mediator was thus added into the electrolyte to further evaluate the orientation of the enzyme at a given pH. In the case of pH 3.6, a clear MET signal can be observed corresponding to 20% of the total catalytic signal. But at the other pHs of adsorption, MET current is either zero or less than 5 % (Figure 2A and Figure 2B, red lines), in accordance with a narrow enzyme distribution.

Catalytic current relative magnitude can be ascribed either to a different amount of loaded enzymes with similar ET rates, or to different ET rates of similar amount of proteins adsorbed. Change in enzyme orientation or modification of enzyme conformation can affect the ET. The appearance of the amide bands at the same wavelength in the PMIRRAS spectra irrespective of the adsorption pH, demonstrates that there is no change in the secondary structure of the enzyme (Figure 2D). Similar values of βd_0 further suggest that the loading of enzymes should be more critical than the orientation of the enzyme. Accordingly, PMIRRAS spectra and SPR signals indicate an increase in the enzyme amount adsorbed on the 6-MHA-SAM with decreasing pHs, which correlates with an increase of the enzyme layer thickness measured by ellipsometry (Figure 2D, Figure 2E and Figure S3). After 15 min of adsorption, values of 2.7±0.39, 6.2±0.89, 10.3±1.5, and 12.2±1.78 pmol.cm^{-2} were obtained from the SPR angle deviations at pH 7.5, 6, 4.6 and 3.6 respectively. Considering that a theoretical monolayer of *Mv* BOD should be between 4.6 and 10.4 pmol.cm^{-2} depending on the conformation the enzyme takes upon immobilization (*Mv* BOD dimensions are 4x5x6 nm^3) [35], a monolayer is not obtained at pH 7.5. More than one monolayer is formed at pH 3.6, which is traduced in an enzyme layer thickness larger than the protein dimension.

Table 1. Values of the parameter βd_0 for distribution of enzyme orientation. Values of βd_0 are obtained from the modeling of CV curves in Figure 2 (adsorption of *Mv* BOD on 6-MHA-SAM at different pHs and electroactivity at pH 6) and Figure 4 (adsorption of *Mv* BOD on 6-MHA-SAM at pH 6 and electroactivity at different pHs). For comparison, βd_0 values obtained by modeling of CVs of O_2 reduction by 20 µM *Mv* BOD adsorbed on bare gold at pH 6 are also given.

pH	Orientation parameter βd_0		
	SAM (6-MHA)		Bare Gold
	Adsorption at different pH	Adsorption at pH 6	Adsorption at pH 6
3.6	5.1 ± 0.15	12.8 ± 0.05	9.6 ± 0.30
4.6	3.9 ± 0.15	10.6 ± 0.12	9.8 ± 0.08
6	4.9 ± 0.19	4.9 ± 0.18	10.9 ± 0.66
7.5	5.1 ± 0.16	6.8 ± 0.17	*

* No DET due to low activity of enzyme

The magnitude of the catalytic current and the loading of enzymes observed as a function of the pH of adsorption can be explained based on the respective charges of the protein, the environment of the CuT1 and the SAM. At pH 7.5, repulsive electrostatic interactions between the negatively charged protein and the negative SAM should prevent BOD adsorption. In accordance, less than one monolayer of enzyme is obtained. Nevertheless, the neutral environment around the CuT1, associated to a high dipole moment (764 Debye) pointing toward the CuT1 [15], enables BOD adsorption via the CuT1. Hence, DET but no MET is observed. The enzyme thickness obtained by ellipsometry (2.7±0.1 nm) (Figure 2E) suggests however some flattening of the enzyme. Compared to pH 7.5, the most prominent change at pH 6 is the lowest negative charge of the SAM. As a consequence, the amount of molecules adsorbed is more than twice higher than at pH 7.5, the enzyme layer thickness is increased (3.3±0.2 nm), leading also to a higher direct catalytic current than when adsorption is made at pH 7.5. At pH 4.6, the amount of adsorbed proteins is enhanced compared to pH 6

because the repulsive interactions are now weak between the protonated SAM and neutral *Mv* BOD. A coverage close to the maximum theoretical coverage is obtained. Ellipsometry gives an enzyme thickness of 3.9±0.2 nm, very close to the geometrical enzyme dimension. The direction of the dipole moment at pH 4.6 which does not point anymore to the T1 should lead to a higher distribution of orientation. However, MET contribution is low, and βd_0 value suggests a narrow distribution of orientation, very similar to pH 6 (Figure 2 and Table 1). Two main hypotheses can be proposed. Either the electrostatic interactions between the Cu T1 and the SAM, although weak, are sufficient to induce a major DET orientation of the enzyme on the surface, or mobility of the protein allows it to adopt a favorable orientation for DET upon transfer to pH 6. The later hypothesis is supported by the increase in the DET current during the first three cycles, before reaching the maximum current as a consequence of progressive reorientation (Figure 2F).

The second main conclusion from our experimental results is that a higher enzyme loading does not translate directly in a higher catalytic activity. The specific activity defined as the ratio of the DET current by the enzyme coverage has been calculated at all the pHs of investigation. It is reported in Figure 3 as a function of the enzyme coverage. This analysis underlines that the highest specific activity is obtained for the lowest coverage. As developed by Blanford and coworkers [36], less steric hindrance because of lower coverage may be the reason for a higher specific activity.

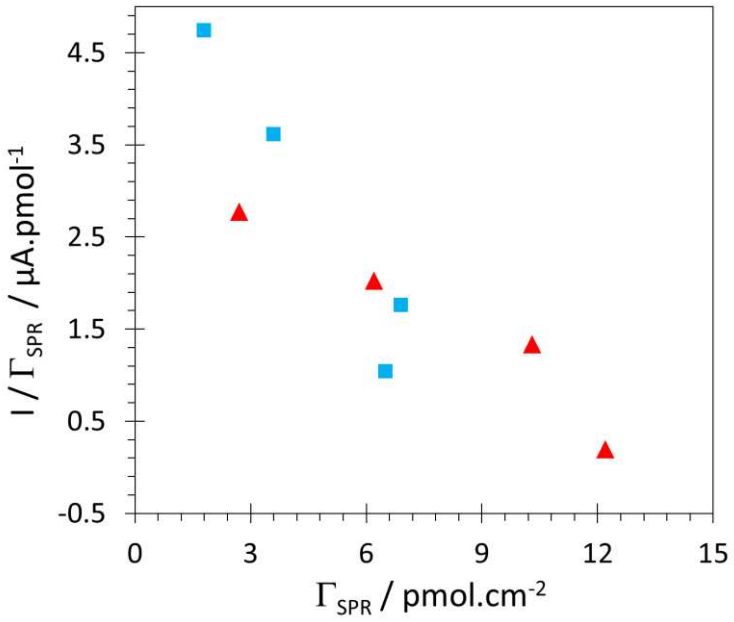

Figure 3. Relation between enzyme coverage and electroactivity. Dependence of the specific enzyme electroactivity on the enzyme coverage after 1 min (■) or 15 min (▲) of *Mv* BOD adsorption. Enzyme coverage is obtained from the SPR angle at the different pHs at RT, catalytic currents are measured at 0 V vs Ag/AgCl at pH 6 and RT. The enzyme adsorption for electrochemistry was made at 4°C.

The case of pH 3.6 is noteworthy to be discussed apart from the other investigated pHs. At this pH, the weak interaction between the positively charged enzyme and the protonated SAM, in addition to a much lower dipole moment (477 Debye) is expected to yield a high degree of mobility of the enzyme, which can adopt many orientations. Although this is the only case where MET contributes to the whole catalytic signal (Figure 2), DET remains the major process, and βd_0 value reflects a narrow distribution of orientations (Table 1). Protein dynamics upon transfer of the bioelectrode from pH 3.6 to pH 6 may explain a favored DET process. Both the amount of protein and the layer thickness measured by ellipsometry are indicative of the formation of more than one monolayer (Figure 2E). The occurrence of a MET process at pH 3.6 can thus be attributed to enzyme multilayers rather than to a

distribution of orientation. Despite the highest amount of proteins, the lowest catalytic current is obtained. The stability of the enzyme is also the lowest at this pH, as highlighted by the homogeneous activity reported in Figure S4, where only 20% of the activity is recovered after 1 hour of storage. Acidic pH conditions, mostly below pH 3, are known to cause protein unfolding as a result of intramolecular charge repulsion [37]. In this work, aggregate formation was effectively observed at pH 3.6 and RT (Figure S5). However, similar enzyme layer thickness values (around 7.2 nm) were obtained by ellipsometry after adsorption at pH 3.6 either at 4°C or at RT, and PMIRRAS spectra indicated that there is no change in the secondary structure of the protein adsorbed at pH 3.6. Thus, aggregation process might not be the major contribution to the low direct catalytic current when adsorption is made at pH 3.6, which would be more related to steric hindrance between proteins in the layer. Interestingly, when adsorption was made at RT at pH 3.6, conditions favoring protein aggregation, the direct electrochemical signal magnitude recorded at pH 6 was four times higher than when the adsorption was made at 4°C (Figure S5). Although it is reported that cross-linked enzyme aggregates (CLEA) of laccases may remain active and stable [38], control experiments in this work showed that unfolded or denaturated proteins do not induce any electrocatalytic signals (Figure S6 and Figure S7). The following hypotheses could thus explain this particular behavior: (i) protein aggregation occurring at RT might remove some BOD population not well folded, and consequently increases the specific catalytic electroactivity, (ii) the presence of aggregated proteins adsorbed on the electrode could optimize the enzyme wiring, playing the role of cross-linkers

.

Varying the pH of electroactivity. The adsorption of *Mv* BOD on 6-MHA-SAM was alternatively carried out at pH 6 for 15 min at 4°C, then the *Mv* BOD/6-MHA-SAM was transferred to buffers at the different pHs 3.6, 4.6, 6 or 7.5, respectively. The typical CVs for

electroenzymatic O_2 reduction are shown in Figure 4A where both DET and MET signals are overlaid.

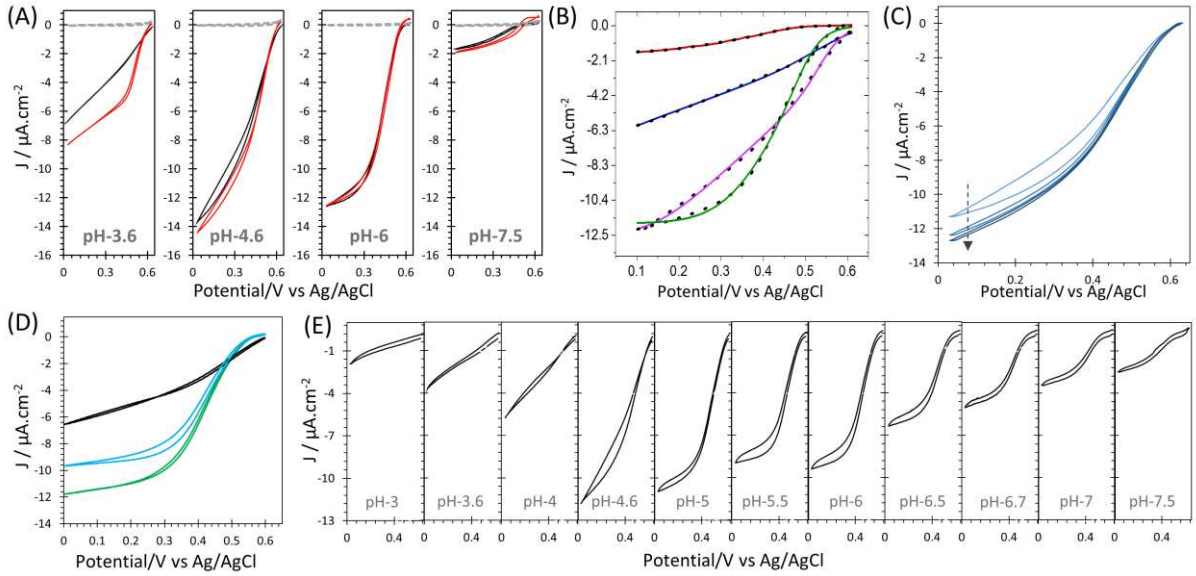

Figure 4. pH-induced dynamics of *Mv* BOD on 6-MHA-SAM. (A) CVs of O_2 reduction by 20 µM *Mv* BOD adsorbed on 6-MHA-SAM at 4°C and pH 6 for 15 min and transferred to different pHs for catalysis measurement (black curves). Red curves are obtained after 50 µM ABTS addition, and grey dotted curves correspond to the SAM alone; (B) Modeling of the electrochemical signal. Electrocatalytic CV curves at different pHs after adsorption at pH 6 (solid line) and curved fitted according to equation 1 (dotted line) (see experimental section). *Mv* BOD was adsorbed on 6-MHA-SAM at pH 6 and electrochemistry was recorded at different pHs: pH 3.6 (blue), pH 4.6 (purple), pH 6 (green), pH 7.5 (red). (C) Increase in the consecutive CV catalytic currents at pH 4.6 after 20 µM *Mv* BOD was adsorbed on 6-MHA-SAM in pH 6 buffer for 15 min at 4°C. (D) CVs for O_2 reduction by *Mv* BOD adsorbed on 6-MHA-SAM at 4°C after multiple steps of transfers: adsorption at pH 6 for 15 min, measurement at pH 6 (green), washing step then transfer and measurement at pH 3.6 (black), washing step then transfer back to pH 6 (blue); (E) CVs of direct O_2 reduction on a full pH range by 20 µM *Mv* BOD adsorbed at pH 6 during 15 min at 4°C. Phosphate citrate buffer (pH 3 to 5.5) or phosphate buffer (pH 6 to 7.5). v = 5 $mV.s^{-1}$.

Switching the pH of the electrolyte changes simultaneously two parameters, i.e. the intrinsic activity of the enzyme as well as the interaction between *Mv* BOD pre-adsorbed at pH 6 and the SAM. A first observation is that the catalytic current mainly reflects the activity of the enzyme in solution measured by UV-Vis spectroscopy (Figure S4). Hence, much lower activity is obtained at pH 7.5 compared to the other pHs. As expected, the onset for O_2 reduction decreases as pH increases displaying a slope close to 60 mV. The second observation is that the shape of the CV curve is markedly different at pH 3.6 and 4.6 compared to pH 6 and 7.5, suggesting a larger distribution of ET rates, linked to a distribution of enzyme orientation. The modeling of the CV curves gave access to the orientation parameter βd_0, which takes values of 12.8, 10.6 and 4.9 for pH 3.6, 4.6 and 6 respectively, showing a large distribution of orientation at pH 3.6 and pH 4.6, and a narrow one at pH 6 (Figure 4B and Table 1). In accordance, MET currents were only observed at pH 3.6 and 4.6, although it cannot be excluded that the magnitude of the MET signal reflects the better affinity of BOD towards ABTS at low pH [39], as attested by the decrease of the Michaelis-Menten constant (Figure S8). These results can be explained based on the weak interactions between the SAM and the protein at acidic pHs as discussed above. But this implies also some mobility of the enzyme when transferring the bioelectrode from pH 6 to lower pHs. Accordingly, the catalytic current increased during the first three cycles before reaching the maximum current (Figure 4C). Protein dynamics is further confirmed by experiments involving multiple transfer steps from one pH to another pH. As seen in Figure 4D, the changes in the CV shapes and current magnitude clearly reflect the reversible changes in the distribution of orientation between pH 6 and pH 3.6. Little less current output at the end of the process could be related to loss of some enzymes in the successive transferring steps. The full range of pH was finally investigated after *Mv* BOD adsorption at pH 6, showing that the electrochemical response can be easily tuned and reflects enzyme activity and dynamics

yielding favorable/unfavorable interaction between the enzyme and the SAM layer for DET (Figure 4E).

Influence of the SAM chemistry. To confirm the electrostatic model established from the electrocatalysis on 6-MHA-SAM, we performed adsorption of *Mv* BOD on other surfaces: (i) 11-MUA-SAM, a carboxylic-thiol with 11 carbons in the alkane chain (pKa of 11-MUA on SAM has been reported to be 6), and (ii) 4-ATP, an amino-thiol. After *Mv* BOD adsorption at pH 6 on 11-MUA-SAM, a DET process is observed when the activity is measured at pH 6, with a lower ET rate than on 6-MHA-SAM, as a consequence of the decrease of the electron tunneling rate with the length of the alkane-chain [40] (Figure S9). As the chemical functions are identical on 11-MUA and 6-MHA, the charges as a function of pH are also similar. Then, the occurrence of DET over MET process on 11-MUA is based on the same assumption as for 6-MHA.

The pKa of 4-ATP was reported to be 6.9. Hence, the SAM is positively charged at pH 3.6, 4.6 and 6, and neutral at pH 7.5. Except at pH 3.6, electrostatic interactions with the globally negatively charged *Mv* BOD must favor enzyme approach. As revealed by the SPR data and confirmed by PMIRRAS and ellipsometry measurements (Table 2, Figure 5A and Figure 5B), *Mv* BOD is adsorbed at pH 6 or at pH 4.6 on 4-ATP-SAM, with similar amounts, reaching a full coverage after 15 min of adsorption. As expected, the amount of loaded enzyme is the lowest at pH 7.5 as a result of lower electrostatic interactions, but higher than on 6-MHA-SAM where repulsive interactions took place. A high amount of proteins is loaded at pH 3.6 despite repulsive interactions which may be ascribed to some aggregation process. The band corresponding to the amide I on the PMIRRAS spectra is slightly shifted toward higher wave numbers in comparison with the adsorption on 6-MHA-SAM (Figure 5B). This change can be

ascribed to a small opening of the β-sheets that become turn, and suggests, as in the case of pH 7.5 on 6-MHA-SAM, that stronger electrostatic interactions may destabilize the enzyme.

Table 2. SPR data for different pH of *Mv* BOD adsorption during 15 min on 4-ATP, and values of the ratio DET/DET+MET at different pHs. The ratios are measured at E = + 120 mV vs Ag/AgCl.

pH of ads.	4-ATP			
	Γ_{SPR} / pmol.cm^{-2}	$I_{DET}/I_{DET+MET}$		
		pH 3.6	pH 4.6	pH 6
3.6	10.97 ± 1.6	0.10	0.36	0.50
4.6	9.5 ± 1.4	0.04	0.23	0.31
6	8.0 ± 1.2	0.06	0.30	0.58
7.5	5.7 ± 0.8	0.38	0.80	0.97

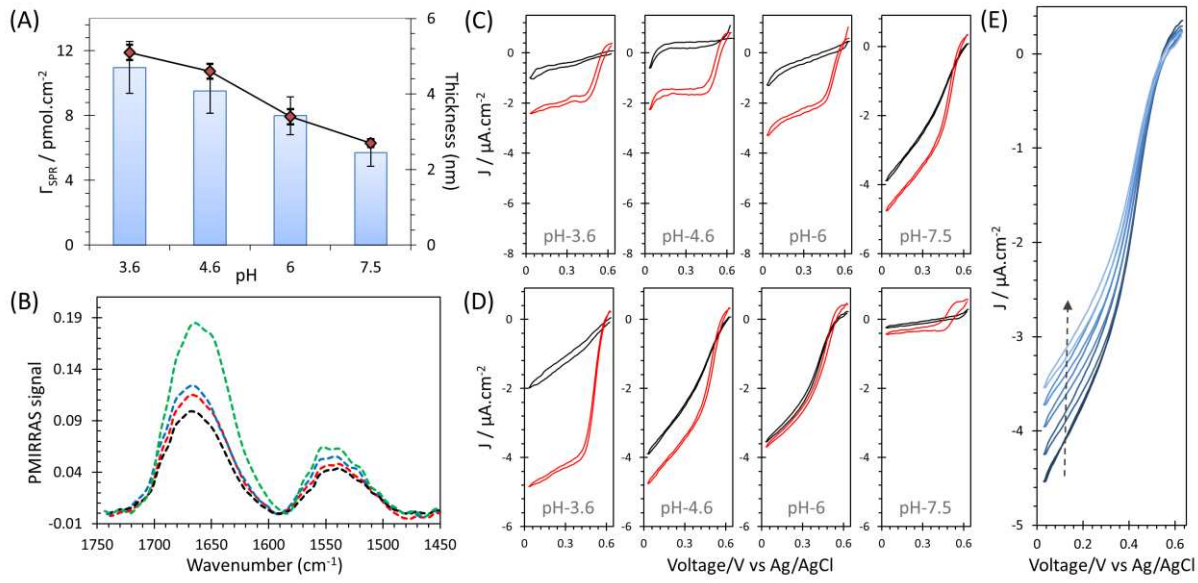

Figure 5. Correlation between electroactivity, conformation and loading of *Mv* BOD adsorbed on amino-based SAM. (A) Enzyme coverage obtained by SPR (blue bars) and enzyme layer thickness obtained by ellipsometry (◆) on 4-ATP-SAM as a function of pH after 15 min of adsorption of 20 µM *Mv* BOD at RT; (B) PMIRRAS spectra of *Mv* BOD adsorbed on 4-ATP-SAM. The gold modified electrode was placed in solution of 20 µM *Mv* BOD at pH 7.5 (black line), pH 6 (blue line),

513 pH 4.6 (red line), and pH 3.6 (green line) during 15 min at 4 °C, and then immersed in phosphate
514 buffer at pH 6 during 30 min at 4°C; Catalytic O_2 reduction (C) at pH 4.6 after *Mv* BOD adsorption in
515 the different pH buffers, or (D) in different pHs after 20 µM *Mv* BOD adsorption at pH 7.5. (E)
516 Decrease in the catalytic current at pH 6 along with CV cycling for bioelectrodes prepared in
517 experiment (D). Black curves and red curves are obtained before and after 50 µM ABTS in solution,
518 respectively. v = 5 $mV.s^{-1}$.

519

520 Figure 5C shows the CVs for O_2 catalytic reduction at pH 4.6 by *Mv* BOD adsorbed at the
521 different pHs before and after ABTS addition. As a result of the electrostatic model which
522 postulates that the electron transfer process is driven by the positive environment of the CuT1,
523 no DET can be observed when the adsorption is made on the positively charged 4-ATP-SAM
524 at pH 3.6, 4.6 and 6. A MET current develops with a similar magnitude whatever the pH of
525 adsorption, underlining that the total amount of electroactive enzymes is similar (Table 2).
526 Also, in good agreement with the model, a DET signal is obtained at pH 7.5, thanks to
527 dynamics of the protein when transferred to a pH where 4-ATP-SAM is neutral. When the
528 adsorption is made at pH 7.5, DET markedly occurs at pH 6 and pH 4.6 (Figure 5D). This
529 behavior has never been reported before, and underlines the original benefit of the protocol
530 used in this work. The DET catalytic process is not stable with time however, as a result of
531 mobility of the protein upon transfer to pHs where the SAM becomes positively charged
532 (Figure 5E).

533

534 **Catalytic stability and effect of applied potential.** One main issue when dealing with
535 enzyme-based bioelectrodes is the long-term stability. Decrease in electrocatalytic signals
536 may be associated to different phenomena including stability of the enzyme itself, enzyme
537 leakage from the electrochemical interface, changes in orientation and/or in the conformation

of the enzyme in the immobilized state. Recent reports coupling electrochemistry to QCM [41] or SPR [16] established that the decrease of the catalytic signal for O_2 reduction by *Mv* BOD adsorbed on SAM layers, was not linked to enzyme loss from the electrode. Although the electric field effect on bioelectrode efficiency and stability is not well established, some other works concluded that decrease in the catalytic activity could be related to changes of the enzyme layer upon applied potential [41-43].

To evaluate the effect of electrostatic interactions on the stability of the DET signal, we cycled during 45 min at different pHs the bioelectrode built by *Mv* BOD adsorbed at pH 6 on 6-MHA-SAM (Figure 6A).

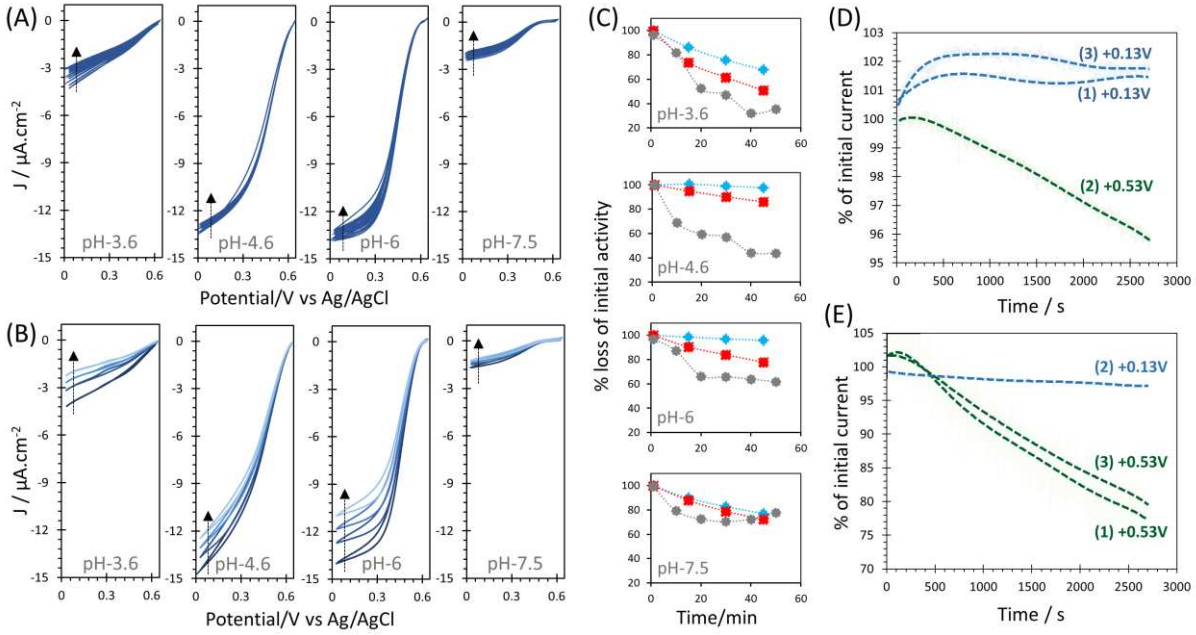

Figure 6. Stability of 6-MHA-SAM/*Mv* BOD, effect of applied potential. Stability of the catalytic O_2 reduction in different pHs by *Mv* BOD adsorbed on 6-MHA-SAM at pH 6 and 4°C during 15 min. (A) continuous CV cycling during 45 min; (B) one cycle every 1000 s holding the electrode at OCP between the cycles; (C) comparative activity loss between (◆) continuous cycling, (■) one cycle every 1000 s and (●) homogeneous catalysis; (D) and (E) effect of applied potential on the stability of the catalytic current. *Mv* BOD adsorbed on 6-MHA-SAM at pH 6, and chronoamperometry recorded at pH 4.6 (D) or pH 6 (E) at +0.13 V (blue lines), or +0.53 V (green lines), with the sequence denoted within brackets.

The percentage of activity loss within 45 min of continuous cycling at RT between 0.6 and 0 V vs Ag/AgCl was 30%, 2%, and 4%, respectively at pH 3.6, 4.6, and 6. Compared to the stability obtained in solution at RT (Figure 6C and Figure S4), enzyme immobilization onto the electrode surface greatly enhances the stability, except in the case of pH 7.5, where heterogeneous or homogeneous catalytic stability is similar (20% against 25%). This latter pH is the case where the repulsive interactions between the enzyme and the SAM are the highest, yielding possible losses of proteins by desorption. SPR measurements confirm this hypothesis as 25% of the adsorbed proteins are removed away after the rinsing step at pH 7.5 against 5% at pH 3.6 and around 10 % at pH 4.6 and 6. But pH 7.5 is also the condition where the electrostatic interactions between the CuT1 and the SAM are the highest. Progressive irreversible change in the structure of the enzyme cannot be excluded as suggested by the higher variability of amide I/amide II ratio in PMIRRAS measurements, and further revealed by the lower thickness obtained by ellipsometry, which suggested some flattening of the enzyme.

The stability of the 6-MHA-SAM/*Mv* BOD biolectrodes apparently differs from the previous measurements that we made on SPR chips at pH 6 [16], where we observed a decrease of more than 30% of the catalytic signal during similar duration. The only difference between the two experiments is that in the current work we are continuously cycling the electrode potential, while in the previous one, we made one cycle every 1000 s and held the electrode at OCP the rest of the time. We used this protocol in the present work, and observed a decrease of the catalytic current of 50%, 15%, 25% and 28%, respectively at pH 3.6, 4.6, 6 and 7.5 (Figure 6B). We undertook comparative chronoamperometry experiments with 6-MHA-SAM modified by *Mv* BOD adsorbed at pH 6 at two different potentials: one situated on the plateau for catalytic O_2 reduction, i.e. + 0.13 V vs Ag/AgCl, and the other close to the OCP, i.e. + 0.53 V vs Ag/AgCl. 4 different pHs (i.e. pH 4.6, 5.5, 6 and 6.5) above and below the pKa of

581 the SAM, and in which the enzyme activity is high and comparable, were studied. In the pH
582 range investigated, the electrostatic interactions between *Mv* BOD and the SAM are either
583 weak or repulsive. Typical curves are provided for the bioelectrodes transferred to pH 4.6
584 (Figure 6D) or pH 6 (Figure 6E).
585 A first observation is that the catalytic signals are more stable at pH 4.6, a condition where
586 both the SAM and the enzyme are neutral. The second main conclusion is that the activity loss
587 is much lower at the lowest applied potential (Table S3). The zero charge potential of the 6-
588 MHA-SAM reported in the literature is E_{pzc} = + 0.116 V vs Ag/AgCl, thus a value close to the
589 lower applied potential in this work, and much lower than OCP [44]. This implies that when
590 applying a potential of + 0.53 V, the electrode surface charge is high and induces a strong
591 electric field. Taken together, this underlines that strong electrostatic interactions destabilizes
592 the *Mv* BOD bioelectrode.

593

594 **CONCLUSION**

595 The practical use of devices such as biosensors, bioreactors or biofuel cells based on redox
596 enzyme activity, relies on the controlled, efficient and stable immobilization of the protein on
597 solid conductive supports. The results obtained in this work provide key parameters to
598 propose new solutions to improve the process. Thanks to a multidisciplinary approach
599 coupling electrochemistry to SPR, ellipsometry and PMIRRAS, we have demonstrated the
600 correlation between enzyme loading, conformation and catalytic activity. The results have
601 been rationalized according to an electrostatic model, where the global charge of the protein
602 influences the rate of adsorption, while the enzyme dipole moment and the charge in the
603 vicinity of the CuT1, the entry site of electrons, influences the enzyme orientation, then the
604 electron transfer rate. We have also demonstrated that strong electrostatic field on the
605 electrode boundary at potentials far from zero-point charge deteriorates enzyme stability.

606 Whether this is a general rule for enzymes on electrochemical interfaces, and whether this
607 could induce changes in the enzyme conformation should be an interesting matter of future
608 discussion.
609 One objective of this work was to evaluate to which extent the hypothesis and main
610 conclusions made on planar surfaces can be extended to porous carbon nanotube networks [15,
611 45]. Actually, Mazurenko *et al.* studied the consequences of BOD adsorption on carbon
612 nanotubes presenting different surface chemistry on the electrocatalytic activity. The
613 experiments conducted in the current work show that the main parameters for enzyme
614 orientation for direct electrical wiring which are determined on planar electrodes are
615 conserved on carbon nanotube networks. That means that rationalization of other enzyme-
616 based bioelectrodes should be gained by the examination of enzyme behavior on planar
617 electrodes taking mainly into account dipole moments, both the direction and value, and the
618 environment of the entry/exit site of electrons on the protein. However, we have also
619 highlighted in this work the dynamics of the protein on SAM-gold electrodes upon changes in
620 the local pH environment which affects the efficiency of the catalysis. Even if immobilization
621 on a porous material with multiple points of contact should restrict protein mobility, our
622 results provide one explanation of the low efficiency of redox proteins in most biodevices.
623 Local variation of pH occurs in the course of electrocatalysis, and the effect on enzyme
624 conformation, stability or orientation in the immobilized state require in-depth investigations,
625 using combination of techniques [46-47]. This will open avenues towards new material and
626 architecture design to protect enzymes against local pH variation.
627
628 **SUPPORTING INFORMATION CONTENT**

629 CV catalytic signal as a function of sweep rate (Figure S1); pKa determination of 6-MHA-SAM
630 (Figure S2); SPR angle variation as a function of pH (Figure S3); homogeneous activity at RT or 4°C

as a function of pH (Figure S4); temperature and pH dependency of *Mv* BOD aggregation (Figure S5); Control experiments using unfolded and denaturated BOD (Figures S6 and S7); electrochemical behavior of ABTS and Mickaelis constant determination (Figure S8); Electrocatalysis on 11-MUA (Figure S9) ant butanethiol (BT) (Figure S10, Table S1); Control experiments on 6-MHA-SAMs (Figure S11); Effect of *Mv* BOD concentration on the electrocatalytic activity (Figure S12 and Table S2); electroactivity loss with time as a function of applied potential at different pH (Table S3). This information is available free of charge on the ACS Publication website.

AUTHOR CONTRIBUTION

Corresponding Author

*e-mail for E.L.: lojou@imm.cnrs.fr

V.P.H. has done the electrochemistry, homogeneous enzyme activity measurements and ellipsometry experiments, and contributed to the redaction of the manuscript. I.M. initiated the modeling of the electrochemical curves. R.C. was in charge of protein purification, and protein modeling. M.T. made the PMIRRAS experiments, and S.C. and S.L. made the PMIRRAS analysis. D.D. made the ellipsometry analysis. M.I. realized the aggregation experiments and analysis of the data. I.M., M.I. and A.P. participated to the discussion of the results. E.L is the initiator and director of the project and participated in all steps.

Competing financial interests

The authors declare no competing financial interests.

ACKNOWLEDGMENT

This work was supported by ANR (ENZYMOR-ANR-16-CE05- 0024), Région PACA (Optolen Project) and Aix-Marseille University for V. Hitaishi's funding. The authors want to thank L. Zuily (BIP, CNRS Marseille) for technical support in protein aggregation characterization. They would like to thank Dr M. Guiral and Dr M.T. Giudici-Orticoni (BIP-CNRS, Marseille) for fruitful discussion, and Y. Malier, J-J. Simon and L. Escoubas for their

useful advises and expertise on the field of ellipsometry. Amano Company is also thanked for the kind gift of BOD.

REFERENCES

1. Kulkarni, A.; Siahrostami, S.; Patel, A.; Norskov, J. K., Understanding Catalytic Activity Trends in the Oxygen Reduction Reaction. *Chemical Reviews* **2018,** *118*, 2302-2312.
2. Xiong, Y.; Yang, Y.; DiSalvo, F. J.; Abruna, H. D., Pt-Decorated Composition-Tunable Pd-Fe@Pd/C Core-Shell Nanoparticles with Enhanced Electrocatalytic Activity toward the Oxygen Reduction Reaction. *Journal of the American Chemical Society* **2018,** *140*, 7248-7255.
3. Holewinski, A.; Idrobo, J. C.; Linic, S., High-performance Ag-Co alloy catalysts for electrochemical oxygen reduction. *Nature Chemistry* **2014,** *6*, 828-834.
4. Mukherjee, S.; Mukherjee, A.; Bhagi-Damodaran, A.; Mukherjee, M.; Lu, Y.; Dey, A., A biosynthetic model of cytochrome c oxidase as an electrocatalyst for oxygen reduction. *Nature Communications* **2015,** *6*, 8467.
5. Mano, N.; de Poulpiquet, A., O_2 Reduction in Enzymatic Biofuel Cells. *Chemical reviews* **2017,** *118*, 2392-2468.
6. Mazurenko, I.; Wang, X.; de Poulpiquet, A.; Lojou, E., H_2/O_2 enzymatic fuel cells: from proof-of-concept to powerful devices. *Sustainable Energy & Fuels* **2017,** *1*, 1475-1501.
7. de Poulpiquet, A.; Kjaergaard, C. H.; Rouhana, J.; Mazurenko, I.; Infossi, P.; Gounel, S.; Gadiou, R.; Giudici-Orticoni, M. T.; Solomon, E. I.; Mano, N.; Lojou, E., Mechanism of Chloride Inhibition of Bilirubin Oxidases and Its Dependence on Potential and pH. *Acs Catalysis* **2017,** *7*, 3916-3923.
8. de Poulpiquet, A.; Marques-Knopf, H.; Wernert, V.; Giudici-Orticoni, M. T.; Gadiou, R.; Lojou, E., Carbon nanofiber mesoporous films: efficient platforms for bio-hydrogen oxidation in biofuel cells. *Physical Chemistry Chemical Physics* **2014,** *16*, 1366-1378.
9. Mazurenko, I.; de Poulpiquet, A.; Lojou, E., Recent developments in high surface area bioelectrodes for enzymatic fuel cells. *Current Opinion in Electrochemistry* **2017,** *5*, 74-84.
10. Sakai, K.; Xia, H.; Kitazumi, Y.; Shirai, O.; Kano, K., Assembly of direct-electron-transfer-type bioelectrodes with high performance. *Electrochimica Acta* **2018,** *271*, 305-311.
11. Lisdat, F., Trends in the layer-by-layer assembly of redox proteins and enzymes in bioelectrochemistry. *Current Opinion in Electrochemistry* **2017,** *5*, 165-172.
12. Mazurenko, I.; Monsalve, K.; Infossi, P.; Giudici-Orticoni, M. T.; Topin, F.; Mano, N.; Lojou, E., Impact of substrate diffusion and enzyme distribution in 3D-porous electrodes: a combined electrochemical and modelling study of a thermostable H_2/O_2 enzymatic fuel cell. *Energy & Environmental Science* **2017,** *10*, 1966-1982.
13. Al-Lolage, F. A.; Meneghello, M.; Ma, S.; Ludwig, R.; Bartlett, P. N., A flexible method for the stable, covalent immobilization of enzymes at electrode surfaces. *ChemElectroChem* **2017,** *4*, 1528-1534.
14. Hitaishi, V. P.; Clement, R.; Bourassin, N.; Baaden, M.; de Poulpiquet, A.; Sacquin-Mora, S.; Ciaccafava, A.; Lojou, E., Controlling Redox Enzyme Orientation at Planar Electrodes. *Catalysts* **2018,** *8*, 192.
15. Mazurenko, I.; Monsalve, K.; Rouhana, J.; Parent, P.; Laffon, C.; Goff, A. L.; Szunerits, S.; Boukherroub, R.; Giudici-Orticoni, M.-T. r. s.; Mano, N., How the intricate

interactions between carbon nanotubes and two bilirubin oxidases control direct and mediated O_2 reduction. *ACS applied materials & interfaces* **2016,** *8*, 23074-23085.
16. Gutierrez-Sanchez, C.; Ciaccafava, A.; Blanchard, P. Y.; Monsalve, K.; Giudici-Orticoni, M. T.; Lecomte, S.; Lojou, E., Efficiency of Enzymatic O_2 Reduction by *Myrothecium verrucaria* Bilirubin Oxidase Probed by Surface Plasmon Resonance, PMIRRAS, and Electrochemistry. *ACS Catalysis* **2016,** *6*, 5482-5492.
17. Gentil, S.; Carriere, M.; Cosnier, S.; Gounel, S.; Mano, N.; Le Goff, A., Direct Electrochemistry of Bilirubin Oxidase from Magnaporthe orizae on Covalently-Functionalized MWCNT for the Design of High-Performance Oxygen-Reducing Biocathodes. *Chemistry-a European Journal* **2018,** *24*, 8404-8408.
18. Blout, A.; Billon, F.; Calers, C.; Methivier, C.; Pailleret, A.; Perrot, H.; Jolivalt, C., Orientation of a Trametes versicolor laccase on amorphous carbon nitride coated graphite electrodes for improved electroreduction of dioxygen to water. *Electrochimica Acta* **2018,** *277*, 255-267.
19. Hoarau, M.; Badieyan, S.; Marsh, E. N. G., Immobilized enzymes: understanding enzyme - surface interactions at the molecular level. *Organic & Biomolecular Chemistry* **2017,** *15*, 9539-9551.
20. Rodrigues, R. C.; Ortiz, C.; Berenguer-Murcia, A.; Torres, R.; Fernandez-Lafuente, R., Modifying enzyme activity and selectivity by immobilization. *Chemical Society Reviews* **2013,** *42*, 6290-6307.
21. Chumillas, S.; Maestro, B.; Feliu, J. M.; Climent, V., Comprehensive Study of the Enzymatic Catalysis of the Electrochemical Oxygen Reduction Reaction (ORR) by Immobilized Copper Efflux Oxidase (CueO) From *Escherichia coli*. *Frontiers in Chemistry* **2018,** *6*, 358.
22. Yang, S. J.; Liu, J.; Quan, X. B.; Zhou, J., Bilirubin Oxidase Adsorption onto Charged Self-Assembled Monolayers: Insights from Multiscale Simulations. *Langmuir* **2018,** *34*, 9818-9828.
23. Harris, T.; Heidary, N.; Kozuch, J.; Frielingsdorf, S.; Lenz, O.; Mroginski, M. A.; Hildebrandt, P.; Zebger, I.; Fischer, A., In Situ Spectroelectrochemical Studies into the Formation and Stability of Robust Diazonium-Derived Interfaces on Gold Electrodes for the Immobilization of an Oxygen-Tolerant Hydrogenase. *Acs Applied Materials & Interfaces* **2018,** *10*, 23380-23391.
24. Krzeminski, L.; Cronin, S.; Ndamba, L.; Canters, G. W.; Aartsma, T. J.; Evans, S. D.; Jeuken, L. J. C., Orientational Control over Nitrite Reductase on Modified Gold Electrode and Its Effects on the Interfacial Electron Transfer. *Journal of Physical Chemistry B* **2011,** *115*, 12607-12614.
25. Climent, V.; Fu, Y. C.; Chumillas, S.; Maestro, B.; Li, J. F.; Kuzume, A.; Keller, S.; Wandlowski, T., Probing the Electrocatalytic Oxygen Reduction Reaction Reactivity of Immobilized Multicopper Oxidase CueO. *Journal of Physical Chemistry C* **2014,** *118*, 15754-15765.
26. Jin, B.; Wang, G.-X.; Millo, D.; Hildebrandt, P.; Xia, X.-H., Electric-field control of the pH-dependent redox process of cytochrome c immobilized on a gold electrode. *The Journal of Physical Chemistry C* **2012,** *116*, 13038-13044.
27. Hexter, S. V.; Esterle, T. F.; Armstrong, F. A., A unified model for surface electrocatalysis based on observations with enzymes. *Physical Chemistry Chemical Physics* **2014,** *16*, 11822-11833.
28. Rakic, A. D.; Djurisic, A. B.; Elazar, J. M.; Majewski, M. L., Optical properties of metallic films for vertical-cavity optoelectronic devices. *Applied Optics* **1998,** *37*, 5271-5283.
29. Voros, J., The density and refractive index of adsorbing protein layers. *Biophysical Journal* **2004,** *87*, 553-561.

30. Utesch, T.; Millo, D.; Castro, M. A.; Hildebrandt, P.; Zebger, I.; Mroginski, M. A., Effect of the protonation degree of a self-assembled monolayer on the immobilization dynamics of a [NiFe] hydrogenase. *Langmuir* **2013,** *29*, 673-682.
31. Felder, C. E.; Prilusky, J.; Silman, I.; Sussman, J. L., A server and database for dipole moments of proteins. *Nucleic acids research* **2007,** *35*, W512-W521.
32. Dolinsky, T. J.; Nielsen, J. E.; McCammon, J. A.; Baker, N. A., PDB2PQR: an automated pipeline for the setup of Poisson-Boltzmann electrostatics calculations. *Nucleic Acids Research* **2004,** *32*, W665-W667.
33. Marmisollé, W. A.; Capdevila, D. A.; de la Llave, E.; Williams, F. J.; Murgida, D. H., Self-Assembled Monolayers of NH_2-Terminated Thiolates: Order, pKa, and Specific Adsorption. *Langmuir* **2013,** *29*, 5351-5359.
34. Bryant, M. A.; Crooks, R. M., Determination of surface pKa values of surface-confined molecules derivatized with pH-sensitive pendant groups. *Langmuir* **1993,** *9*, 385-387.
35. Pankratov, D.; Sotres, J.; Barrantes, A.; Arnebrant, T.; Shleev, S., Interfacial behavior and activity of laccase and bilirubin oxidase on bare gold surfaces. *Langmuir* **2014,** *30*, 2943-2951.
36. McArdle, T.; McNamara, T. P.; Fei, F.; Singh, K.; Blanford, C. F., Optimizing the Mass-Specific Activity of Bilirubin Oxidase Adlayers through Combined Electrochemical Quartz Crystal Microbalance and Dual Polarization Interferometry Analyses. *Acs Applied Materials & Interfaces* **2015,** *7*, 25270-25280.
37. Tapley, T. L.; Korner, J. L.; Barge, M. T.; Hupfeld, J.; Schauerte, J. A.; Gafni, A.; Jakob, U.; Bardwell, J. C. A., Structural plasticity of an acid-activated chaperone allows promiscuous substrate binding. *Proceedings of the National Academy of Sciences of the United States of America* **2009,** *106*, 5557-5562.
38. Yamaguchi, H.; Kiyota, Y.; Miyazaki, M., Techniques for Preparation of Cross-Linked Enzyme Aggregates and Their Applications in Bioconversions. *Catalysts* **2018,** *8*, 174.
39. Otsuka, K.; Sugihara, T.; Tsujino, Y.; Osakai, T.; Tamiya, E., Electrochemical consideration on the optimum pH of bilirubin oxidase. *Analytical Biochemistry* **2007,** *370*, 98-106.
40. Smalley, J. F.; Feldberg, S. W.; Chidsey, C. E.; Linford, M. R.; Newton, M. D.; Liu, Y.-P., The kinetics of electron transfer through ferrocene-terminated alkanethiol monolayers on gold. *The Journal of Physical Chemistry* **1995,** *99*, 13141-13149.
41. Singh, K.; McArdle, T.; Sullivan, P. R.; Blanford, C. F., Sources of activity loss in the fuel cell enzyme bilirubin oxidase. *Energy & Environmental Science* **2013,** *6*, 2460-2464.
42. Dagys, M.; Laurynėnas, A.; Ratautas, D.; Kulys, J.; Vidžiūnaitė, R.; Talaikis, M.; Niaura, G.; Marcinkevičienė, L.; Meškys, R.; Shleev, S., Oxygen electroreduction catalysed by laccase wired to gold nanoparticles via the trinuclear copper cluster. *Energy & Environmental Science* **2017,** *10*, 498-502.
43. Sugimoto, Y.; Kitazumi, Y.; Tsujimura, S.; Shirai, O.; Yamamoto, M.; Kano, K., Electrostatic interaction between an enzyme and electrodes in the electric double layer examined in a view of direct electron transfer-type bioelectrocatalysis. *Biosensors and Bioelectronics* **2015,** *63*, 138-144.
44. Smalley, J. F., Potential of Zero Charge and Its Temperature Derivative for Au(111) Electrode vertical bar Alkanethiol SAMI1.0 M Aqueous Electrolyte Solution Interfaces: Impact of Electrolyte Solution Ionic Strength and Its Effect on the Structure of the Modified ElectrodelElectrolyte Solution Interface. *J. Phys. Chem. C* **2017,** *121*, 9260-9272.
45. Hoshikawa, Y.; Castro-Muniz, A.; Tawata, H.; Nozaki, K.; Yamane, S.; Itoh, T.; Kyotani, T., Orientation Control of Trametes Laccases on a Carbon Electrode Surface to

Understand the Orientation Effect on the Electrocatalytic Activity. *Bioconjugate Chemistry* **2018,** *29*, 2927-2935.
46. Zhang, Y. F.; Tsitkov, S.; Hess, H., Proximity does not contribute to activity enhancement in the glucose oxidase-horseradish peroxidase cascade. *Nature Communications* **2016,** *7*, 13982.
47. Lancaster, L.; Abdallah, W.; Banta, S.; Wheeldon, I., Engineering enzyme microenvironments for enhanced biocatalysis. *Chemical Society reviews* **2018,** *47*, 5177-5186.

GRAPHICAL ABSTRACT